Characteristics of Parallel Inverters Applying Virtual Synchronous Generator Control

Chen, Meng; Zhou, Dao; Wu, Chao; Blaabjerg, Frede

Published in:
I E E E Transactions on Smart Grid

DOI (link to publication from Publisher):
10.1109/TSG.2021.3102994

Publication date:
2021

Document Version
Accepted author manuscript, peer reviewed version

Characteristics of Parallel Inverters Applying Virtual Synchronous Generator Control

Meng Chen, *Student Member, IEEE,* Dao Zhou, *Senior Member, IEEE,* Chao Wu, *Member, IEEE,* and Frede Blaabjerg, *Fellow, IEEE*

***Abstract*—The virtual synchronous generator (VSG) is a promising way to deal with the lack of physical inertia and damping introduced by the power-electronic-based power supply system. However, the inertia and damping characteristics may be complicated in a paralleled VSG system due to the lack of a stiff power grid and the interactions between the control system of the inverters. In this paper, the dynamics of parallel inverters with VSGs is studied. The equivalent inertia and damping characteristics are derived and analyzed in detail considering both changing of set-points and load disturbance, where the transient load sharing is also investigated. Furthermore, a better dynamics is achieved by an inertia switching strategy. Experimental results verify the effectiveness of the analysis and the proposed strategy.**

***Index Terms*—Parallel inverters, virtual synchronous generator, equivalent coefficients, transient load sharing.**

I. Introduction

As more converter interfaced generators are integrated into the power system, they are required to participate in the frequency and voltage regulation in order to keep the stable operation of the power system. Droop control has been proved as a solution while achieving power sharing among paralleled units, which mimics the droop mechanism of a traditional governor. Furthermore, in order to eliminate the influence of impedance mismatch and improve the stability of the controller, a virtual impedance control is proposed, which is similar with the windings of a synchronous generator (SG). However, both the droop control and the virtual impedance control cannot provide enough inertia like an SG, which implies that a large rate of change of frequency (RoCoF) and frequency deviation may occur after various disturbances. In an SG, the mechanical rotor can provide large inertia. In comparison, the power electronic converters are static systems without physical inertia, which may harm the frequency performance in the power system [1].

In order to solve the problem caused by the lack of physical inertia, some new strategies including virtual inertia have been proposed in the literature, where the virtual synchronous generator (VSG) has drawn wide attention due to its favorable features. A VSG includes the swing equation of the SG into the control system of the inverter so that the static inverter can operate with inertia characteristics like in an SG [2], [3]. Further, it is easy to achieve the droop characteristics and virtual impedance by emulating the governor and windings, respectively [4]. To highlight the benefits, several works have compared the performance of VSG with droop control such as in [5] and [6]. In a word, a VSG can not only combine the advantages of both droop control and virtual impedance, but also provide additional inertia.

In general, the formal definition of the power system stability with distributed generators (DGs) are identical with the traditional power system, i.e., the ability, for a given initial operation condition, to regain a state of operating equilibrium after a disturbance, with most system variables bounded so that practically the entire system remains intact [7]. Nevertheless, the limitations for some indices are changed. Usually, the RoCoF and frequency deviations can be used to evaluate the frequency stability. According to IEEE Std 1547-2018, the distributed generators should be in continuous operation when the frequency deviations are within ± 1.2 Hz. Besides, the DGs should ride though for at least a 0.5 Hz/s of RoCoF over an averaging window of 0.1 s [8]. In addition, a new limitation of 1 Hz/s is recommended in Ireland for a system with more than 75% of converter-based generators [9]. As the above indices are highly related to the inertia and damping level, it is necessary to investigate these characteristics provided by the inverters in order to understand the dynamics of the system with more power electronic converters. In [10] and [11], the equivalent inertia of a doubly-fed induction generator (DFIG) based wind turbine system and a photovoltaic (PV) system provided by a modified phase-locked loop (PLL) rather than a VSG are investigated, respectively. In [12], the DC-link capacitor in a grid-connected PV system is used to provide the virtual inertia, where the equivalent inertia, damping, and synchronizing coefficients are derived by a torque analysis to represent the characteristics of the PV system. The same method is adapted by [13] to study the VSG. However, it focuses on a grid-connected single machine infinite bus system.

In many applications of the VSG, there is not a robust power grid, and even not a dominant power source such as in a parallel VSGs system, where the dynamics of the VSGs may influence each other [14]. In [15], the robust stability of the parallel VSGs system is studied by using μ-analysis, which reveals the impact of a parallel VSG on the stability margin. However, the parameters impact on the inertia and damping characteristics dynamically are not focused on. A frequency analysis of the parallel VSGs is given in [16] to investigate the inertia interaction among different VSGs, while the value of the equivalent inertia is not studied. Meanwhile, the damping is not considered in this literature. In [17], the index "transient active power circulation (TAPC)" is used to

The authors are with the Department of Energy Technology, Aalborg University, Denmark. (Corresponding author: Chao Wu.)

study the impact of the parameters on dynamics of the parallel VSGs system, where the way that the parameters will influence a specific VSG can not be reflected. The inertia and damping characteristics of the VSG, which may change due to the interaction with the paralleled one, have not been evaluated in detail either.

In addition, one of the important problems of the parallel VSGs is the transient power sharing, which may lead to large power oscillations. In [18] and [19], an inertia design method and a virtual capacitor control of parallel VSGs are proposed from the point of view of power sharing. Moreover, the power sharing is also related to the damping of the VSG, which is studied in [20]. In [21] and [22] , the conditions to achieve better transient active power sharing is discussed, which shows that the corresponding parameters of the parallel VSGs should be exactly identical in p.u. values. A similar work is given in [23], where the same voltage magnitudes are required. However, the voltages, which are changeable with the reactive power of the system, are not constant during the operation.

In our previous research in [24], a single VSG system with local loads connected into an ideal grid is investigated. As an extension, this paper considers a parallel VSGs system without a stiff grid. Therefore, the main purpose is to investigate how the paralleled units will influence the dynamics of each other. Meanwhile, it will be proved that the results in [24] can be seen as a special case of this paper. In addition, [24] only addresses the load disturbance. However, variations in the set-point value as well as the impact of a dedicated damping term will also be considered in this paper.

In this paper, an equivalent coefficients model is built and used to investigate the inertia and damping characteristics of the parallel VSGs system. Meanwhile, unlike the stability analysis based on the characteristic equation, the impacts of the input signal, which influences the closed-loop zeros, on the dynamics are also considered. Based on the derived equivalent coefficients model, a more general condition to achieve the transient power sharing is obtained easily. Then to achieve better performance with a variation of the set-point value, a simple inertia switching strategy based on the set-point value of the active power is proposed for the parallel VSGs system. Although some damping strategies can be used to decrease the power oscillation, they are more complicated due to more control parameters [22], [25], [26]. In [27]–[29], several alternating inertia control strategies are proposed as well. However, the inertia switching is based on the frequency and will occur with any disturbance, which influence the transient power sharing during a load step. Meanwhile, they are hard to work in the parallel VSGs system, which may have a frequency deviation in steady-state operation.

As a result, the contributions of this paper are summarized as follows.

1) The equivalent coefficients of the parallel VSGs under load disturbance and set-point changing are derived. The results reveal which parameters and how they will influence the dynamics of the VSGs in a parallel system.
2) Based on the derived equivalent coefficients, the conditions for achieving transient power sharing are easily derived, which is an extension of the results in [21] and [23]. It shows that the corresponding parameters are not necessarily identical between the parallel VSGs even in p.u. values.
3) A simple enhanced inertia control strategy based on the set-value of the active power is proposed to achieve good performance of frequency under both conditions of load disturbances and set-point changing.

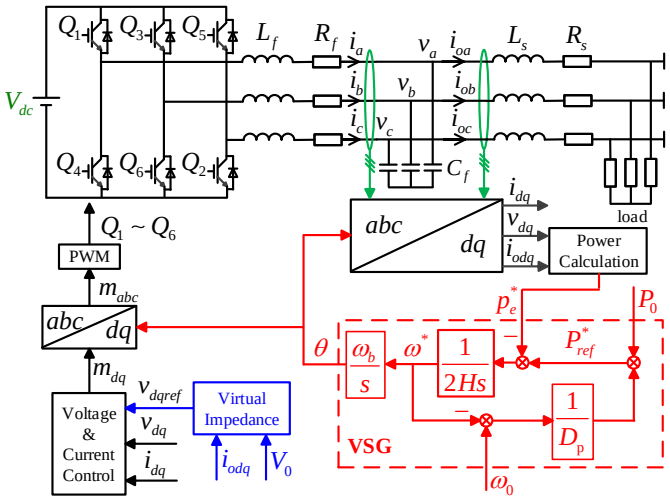

Fig. 1. Topology and control of VSG with a constant DC source (V_{dc}).

The rest of paper is organized as follows. The basic principle of VSG and its control is presented in Section II. In Section III, a small-signal model of the parallel VSGs system is established and used to investigate the inertia and damping characteristics. The transient power sharing is considered as well. In Section IV, a modified inertia is proposed to improve the performance of the VSG. Experimental results are shown in Section V, and conclusions are drawn in Section VI.

II. Virtual Synchronous Generator and Its Control

Fig. 1 shows the topology and the control diagram of the VSG, where L_f, R_f, and C_f are the filter inductance, the equivalent resistance of the filter inductor, and the filter capacitance. L_s and R_s represent the inductance and resistance of the line to the load. The three-phase currents of the filter inductor, i_{abc}, the three-phase output voltages and currents, v_{abc} and i_{oabc}, are measured as the inputs of the control system. The VSG emulates the swing equation of the SG, which is

$$\begin{cases} P_{ref}^* - p_e^* = 2H\dfrac{d\omega^*}{dt} \\ \dfrac{d\theta}{dt} = \omega^*\omega_n \end{cases} \tag{1}$$

where the superscript "*" represents the p.u. value. P_{ref} and p_e are the input and output power, ω and ω_n are the virtual angle speed of the rotor and its nominal value, and θ is the rotor angle, which is used for the coordinate frame transform, and, thus, the use of a PLL is avoided. H is the inertia constant.

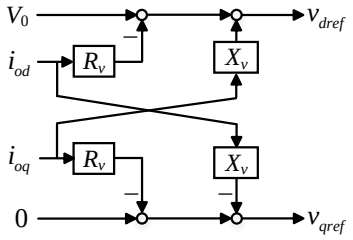

Fig. 2. Block diagram of virtual impedance.

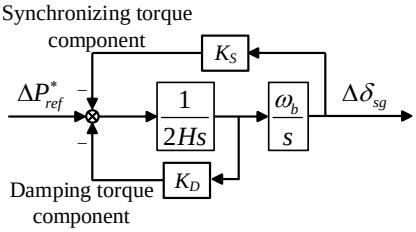

Fig. 3. Equivalent coefficients model used in analysis of traditional power system [30].

As shown in Fig. 1, to guarantee power sharing between multiple VSGs, the droop control emulating the governor is implemented into the VSG control, which is

$$\omega_0 - \omega^* = D_p(P^*_{ref} - P_0) \tag{2}$$

where "0" represents the set-point, D_p is the droop coefficient. Due to the decoupling between the active and reactive power, the $Q-V$ droop is not considered in this paper.

For the VSG using a double-loop control strategy, the virtual impedance is normally used to decouple the active and reactive power, and enhance the stability of the system. Fig. 2 shows the block diagram of the virtual impedance, which can influence the references v_{dqref} for the inner loops using the output currents i_{odq}. Its mathematical expression is given by (3).

$$v_{dref} + jv_{qref} = V_0 - (R_v + jX_v)(i_{od} + ji_{oq}) \tag{3}$$

where R_v and X_v are the virtual resistance and virtual reactance, respectively.

III. Characteristics of Parallel Virtual Synchronous Generator

A. Equivalent coefficients analysis of SG model

In the traditional power system, the dynamics of the frequency mainly relies on the influence of the torque unbalance and the rotational inertia, which can be investigated using an equivalent coefficients model as shown in Fig. 3 [12], [13], [30]. As seen, this model determines the dynamics from four factors, i.e., the input signal, the inertia, the synchronizing torque component, and the damping torque component. The input signal represents the characteristics of the disturbance, the inertia is related to the RoCoF, the synchronizing torque component is related to the aperiodic oscillation, and the damping torque component is related to the periodic oscillation.

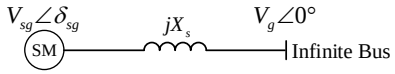

Fig. 4. General diagram of single machine infinite bus system where SM is a synchronous generator.

Usually, for the stability analysis of the traditional power system, it is supposed that the SG is connected into an infinite bus without the local load as shown in Fig. 4. Therefore, the input power ΔP^*_{ref} is chosen as the input signal, which leads to

$$K_J = 2H \tag{4}$$

where K_J is the equivalent inertia coefficient. As seen, the equivalent inertia is only determined by the inertia constant of the rotor, and all other influences from the system will be reflected in the synchronizing torque and damping torque components. In this context, the equivalent synchronizing and damping coefficients, i.e., K_S and K_D will be different according to the governor, impedance, etc.

However, a parallel VSGs system has two main differences compared to the system show in Fig. 4. First, a local load can also be the disturbance of the system. Second, there is not an infinite bus in this islanded system. Therefore, the corresponding equivalent coefficients model may be quite different as well.

B. Small-signal model of parallel VSGs

There are two set-point values in Fig. 1, i.e., P_0 and ω_0. This paper uses P_0 as an example to investigate the characteristics when there is a variation in the set-point value. The impact of ω_0 can be analyzed similarly because the only difference between them is D_p as shown in Fig. 1.

The studied parallel VSGs system is shown in Fig. 5, where the equivalent circuit is shown in Fig. 6. Although the line in the low voltage usually has a low X/R ratio, it can be solved by the virtual inductance control. It can be seen from Fig. 6 that the virtual inductance increases the equivalent inductance between the VSG and the load. Fig. 7 shows the comparisons responding to a load step with and without considering the resistance. It is noted that VSG 1 is taken as the example, where $L_s = 1$ mH (0.3 Ω) and $R_s = 2.4$ Ω (the ratio of R/X is assumed to be around 7.7 in a low-voltage network [31]). The virtual reactance of 3 Ω is applied to both VSGs in order to make the equivalent impedances to be inductive. Although the line resistance changes the steady-state due to its voltage drop, the influence is not that significant. More importantly, the resistance does not significantly change the dynamic waveforms. Besides, in practice, there may also be several factors to make the equivalent impedance more inductive and further decrease the impact of the resistance. First, the VSG may be connected into the power grid via an LCL filter and/or an transformer such as in [5] and [32], where the grid-side inductor of the LCL filter and/or the equivalent inductance of the transformer will increase the total equivalent inductance. Second, a higher virtual reactance can be used (e.g., 6 Ω and 9 Ω are used in Section V). Therefore, the line

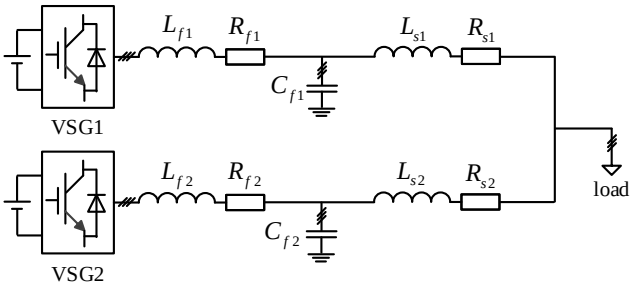

Fig. 5. Topology of parallel VSGs.

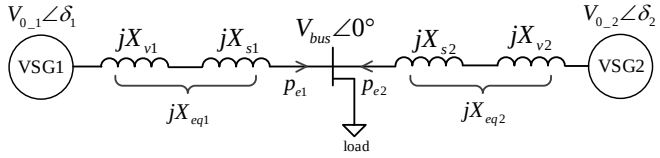

Fig. 6. Equivalent circuit of parallel VSGs shown in Fig. 5.

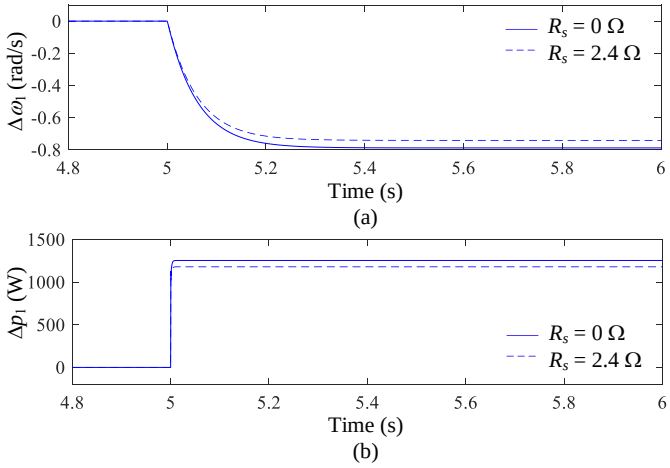

Fig. 7. Comparisons of VSG1 responding to load step with and without considering the line resistance. (a) Variations of angular frequency. (b) Variations of output active power.

resistance is neglect in the following analysis just like in [16] and [21].

Similarly, as shown in Fig. 7(b), the loss of the line does influence the output active power. Nevertheless, it is negligible compared to the load variation and does not change the dynamic waveform remarkably. Thus, it is assumed that the loss of the line is zero in the following analysis. In some topics such as the economic regulation, the losses on the line may become important. However, they can be neglected in this paper. In Section V, the experimental results are in accordance with the conclusion of the analysis, which also verifies that neglecting the loss of the line is reasonable. Thereafter, all the output power of the VSGs is consumed by the load, i.e.,

$$\sum_{i=1,2} \Delta p_{ei}^* = \Delta p_l^* \tag{5}$$

where p_l^* is the active power consumption of the load. It is noted that for a constant load resistance, p_l^* is only determined by the load voltage. However, as in normal operation, the voltage can only change in a narrow area, e.g., 0.95 p.u.-1.05 p.u., the small-signal variation of the load power due to voltage changing is small. Therefore, when discussing a load variation, it usually means a load step, i.e., variation in the load resistance. For an inductive line, the active power is dominated by the angle difference [21].

Define δ_i as the angle separation between the voltages of the VSGi and the load bus, which is calculated by

$$\delta_i = \int (\omega_i^* - \omega_{bus}^*)\omega_n dt \tag{6}$$

Although the double loop and power stage can also influence the stability of the system, their dynamics are usually with relative high frequencies of at least several hundreds Hz [33]. Therefore, when studying the slow dynamics of the power loops with frequencies of only several Hz, the quick dynamics of the double loop and the power stage may be neglected such as in [17] and [19]. Then, the output power can be simplified to

$$p_{ei}^* = \frac{V_{0\_i}V_{bus}}{X_{eqi}S_n}\sin\delta_i \tag{7}$$

where V_{bus} is the voltage of the load bus. The small-signal equations are

$$\Delta p_{ei}^* = \frac{\partial p_{ei}^*}{\partial V_{bus}}\Delta V_{bus} + \frac{\partial p_{ei}^*}{\partial \delta_i}\Delta\delta_i \tag{8}$$

As mentioned before, the impact of ΔV_{bus} on Δp_{ei} is small. Therefore, the upper equation can be simplified to

$$\Delta p_{ei}^* = \frac{\partial p_{ei}^*}{\partial \delta_i}\Delta\delta_i \tag{9}$$

Define two intermediate coefficients as

$$K_1 = \frac{\partial p_{e1}^*}{\partial \delta_1} = \frac{V_{0\_1}V_{bus0}}{X_{eq1}S_n}\cos\delta_{10} \tag{10}$$

$$K_2 = \frac{\partial p_{e2}^*}{\partial \delta_2} = \frac{V_{0\_2}V_{bus0}}{X_{eq2}S_n}\cos\delta_{20} \tag{11}$$

which yields

$$\Delta p_{e1}^* = K_1\Delta\delta_1 \tag{12}$$

$$\Delta p_{e2}^* = K_2\Delta\delta_2 \tag{13}$$

By combining (5), (12), and (13), the output active power of the VSG can be expressed as

$$\Delta p_{e1}^* = \frac{K_1}{K_1+K_2}\Delta p_l^* + \frac{K_1K_2}{K_1+K_2}(\Delta\delta_1 - \Delta\delta_2) \tag{14}$$

$$\Delta p_{e2}^* = \frac{K_2}{K_1+K_2}\Delta p_l^* - \frac{K_1K_2}{K_1+K_2}(\Delta\delta_1 - \Delta\delta_2) \tag{15}$$

Based on the aforementioned analysis, the block diagram of the small-signal model for a parallel VSGs system is shown in Fig. 8. It indicates that although (6) defines δ, the actual independent state variable is the difference between VSG1 and VSG2, i.e., $\Delta\delta_1$-$\Delta\delta_2$.

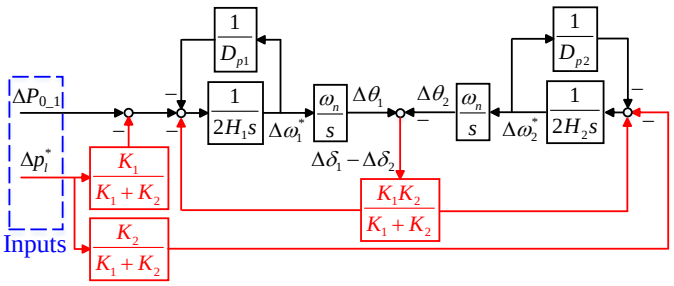

Fig. 8. Small-signal block diagram of parallel VSGs shown in Fig. 5.

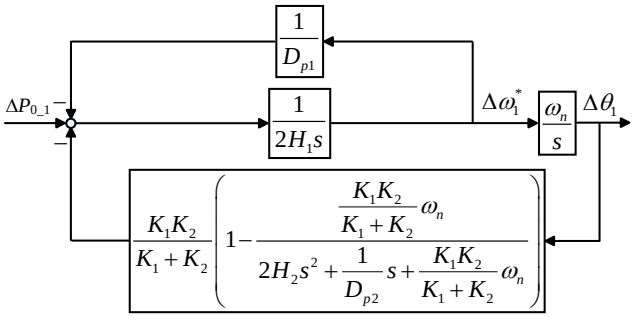

Fig. 9. Equivalent block diagram of parallel VSGs with control input of VSG1.

C. Characteristics Analysis by Equivalent Coefficients

This section gives a similar equivalent coefficients model as shown in Fig. 3, where K_J and K_D represents the equivalent inertia and damping when a disturbance occurs. The other dynamic is represented by K_S. By the equivalent coefficients, it is easy to know which parameters and how they can influence the dynamics of frequency of the VSG. In general, the RoCoF changes inversely with K_J, which implies that a larger K_J can slow down the variation of the frequency when disturbances occur, improve the nadir, and decrease the oscillatory frequency. In comparison, K_D mainly influences the oscillatory magnitude without changing the oscillatory frequency, where a larger K_D usually decreases the overshoot of the response. K_S reflects the impact of the paralleled VSG, which can change the synchronization process in a longer time scale. However, the inertia and damping characteristics (e.g., RoCoF) at the beginning of disturbances are not affected by K_S. Here, both the influence of the control input P_{0_1} and the load disturbance are studied by using VSG1 as an example. The impact of P_{0_2} on VSG1 is not considered in this paper, because P_{0_2} will not introduce closed-loop zeros, and the dynamics is, therefore, exactly determined by the closed-loop poles, which can be analyzed by root loci as given in [21].

1) Characteristics when control input of VSG1 changes: In this case, Δp_l is set to zero, where the equivalent block diagram is simplified to Fig. 9. Therefore, the equivalent coefficients are expressed as

$$\begin{cases} K_J = 2H_1 \\ K_D = \dfrac{1}{D_{p1}} \\ K_S = \dfrac{K_1K_2}{K_1+K_2}\left[1 - \dfrac{K_1K_2\omega_n/(K_1+K_2)}{2H_2s^2 + 1/D_{p2}s + K_1K_2\omega_n/(K_1+K_2)}\right] \end{cases} \tag{16}$$

As seen, when P_{0_1} changes, the equivalent inertia and damping of VSG1 are only determined by H_1 and D_{p1}, respectively, and they are independent on the parameters of VSG2 and the system parameters. In terms of K_S, it is related to the inertia and damping of VSG2, but is independent on the parameters of VSG1. In addition, K_S is influenced by the system parameters K_1 and K_2 as well. It is concluded that, in this case, VSG1 determines the inertia and damping characteristics, while VSG2 influences the dynamics to the steady-state.

It is worth noting that when $H_2 = +\infty$ and $D_{p2} = 0$, VSG2 becomes an ideal source, where K_S is simplified to

$$K_S = \frac{K_1K_2}{K_1+K_2} \tag{17}$$

Considering $X_{eq2} = 0$ further, which leads to $K_2 = +\infty$, (17) becomes

$$K_S = K_1 \tag{18}$$

This is the special case of a single machine infinite bus in the traditional power system.

2) Characteristics when load steps: In this case, ΔP_{0_1} is set to zero, where the equivalent block diagram is simplified to Fig. 10. The equivalent coefficients are expressed as

$$\begin{cases} K_J = 2H_1\dfrac{K_1+K_2}{K_1} \\ K_D = \dfrac{1}{D_{p1}}\dfrac{K_1+K_2}{K_1} \\ K_S = \dfrac{K_2}{K_1H_2}\left[K_2\dfrac{(H_1/D_{p2} - H_2/D_{p1})s + (K_2H_1 - K_1H_2)\omega_n}{2H_2s^2 + (1/D_{p2})s + K_2\omega_n} + K_1H_2 - K_2H_1\right] \end{cases} \tag{19}$$

As seen, when there is a load step, the equivalent inertia of VSG1 is also related to H_1 rather than H_2, which implies that the inertia characteristics will not be influenced by the inertia provided by the paralleled VSG just like the case when P_{0_1} changes. Similarly, the damping of VSG1 is determined by itself rather than the paralleled VSG. Furthermore, K_1 and K_2 will influence the equivalent inertia and damping as well. A larger ratio between K_1 and K_2 leads to smaller equivalent inertia and damping. Meanwhile, parameters of VSG2 will influence the dynamics to the steady-state by changing K_S.

Considering that VSG2 is an ideal source, which means that $H_2 = +\infty$ and $D_{p2} = 0$, (19) is simplified to

$$\begin{cases} K_J = 2H_1\dfrac{K_1+K_2}{K_1} \\ K_D = \dfrac{1}{D_{p1}}\dfrac{K_1+K_2}{K_1} \\ K_S = K_2 \end{cases} \tag{20}$$

Therefore, the result in [24] can be seen as a special case of this paper. When $X_{eq2} = 0$, which leads to $K_2 = +\infty$, (20)

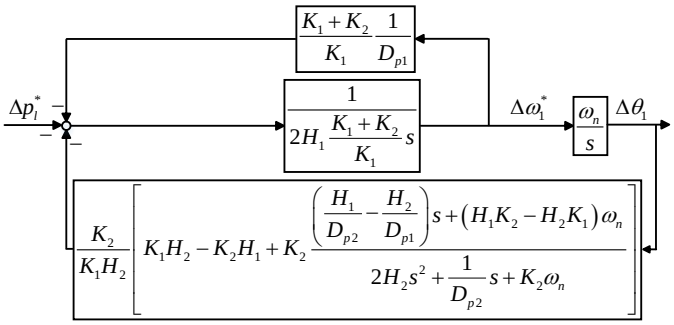

Fig. 10. Equivalent block diagram of parallel VSGs with load step.

becomes

$$\begin{cases} K_J = +\infty \\ K_D = +\infty \\ K_S = +\infty \end{cases} \tag{21}$$

This is because, in this situation, the load is directly connected to an ideal source, which absorbs all the load disturbances, and VSG1 is therefore not influenced.

3) Transient power sharing: When there is a load disturbance, it is recommended that the parallel VSGs should share not only the steady-state load but also the transient load. This requirement can be achieved when all the equivalent coefficients of the parallel VSGs are identical, i.e.,

$$\begin{cases} K_{J1} = K_{J2} \\ K_{D1} = K_{D2} \\ K_{S1} = K_{S2} \end{cases} \tag{22}$$

Combining with (19) yields

$$\frac{H_1}{H_2} = \frac{1/D_{p1}}{1/D_{p2}} = \frac{K_1}{K_2} \tag{23}$$

Therefore, the ratio of the corresponding control parameters are equivalent with each other in order to obtain a good dynamics under the load disturbance. It should be mentioned that, as the model is built in the p.u. system, the condition shown in (23) means the p.u. values.

One of the methods to choose D_{pi} can be based on the capacity of the inverters, which leads to $D_{p1} = D_{p2}$ in p.u. value. Combining with (23) yields $H_1 = H_2$ and $K_1 = K_2$ in this condition. It is noted that, from (10) and (11), K_1 and K_2 have also included the influence of the line impedance. In practice, accurate values of the line impedance are hard to obtain, which implies (23) can scarcely meet exactly. However, it does not change the correctness of (23). Meanwhile, (23) is just an application based on the equivalent coefficients. The conclusions of how the parameters can influence the dynamics in Section III-C are still effective.

4) Impact of dedicated damping term: The studied VSG shown in Fig. 1 has the most basic structure. More complicated VSGs such as the ones with dedicated damping terms can be used. To show their impact on the equivalent coefficients, this paper studies the results with a step of the set-point value using the damping method in [23] and [33] as an example, where the small-signal model of the damping terms p_{di} is

$$\Delta p_{di} = \frac{k_{di}s}{s+\omega_{di}}\Delta\omega_i^* \tag{24}$$

By adding (24) into Fig. 8, (16) becomes

$$\begin{cases} K_J = 2H_1 \\ K_D = \dfrac{1}{D_{p1}} + k_{d1} \\ K_S = \dfrac{K_1K_2}{K_1+K_2}\Big[1 - \dfrac{k_{d1}\omega_{d1}(K_1+K_2)}{K_1K_2\omega_n} + \dfrac{k_{d1}\omega_{d1}^2(K_1+K_2)}{K_1K_2\omega_n(s+\omega_{d1})} \\ \qquad - \dfrac{K_1K_2\omega_n/(K_1+K_2)}{2H_2s^2+(\frac{1}{D_{p2}}+k_{d2})s+\frac{K_1K_2\omega_n}{K_1+K_2}-\frac{k_{d2}\omega_{d2}^2s}{s+\omega_{d2}}}\Big] \end{cases} \tag{25}$$

Comparing (25) with (16) shows that the equivalent inertia coefficients K_J are identical. Therefore, the RoCoF at the beginning is expected not to be changed by the used dedicated damping term. Meanwhile, it is shown that the oscillation can be more damped due to k_{d1} enlarging the equivalent damping coefficient when the disturbance occurs, and the impact of D_{p1} on the damping is not changed. This conclusion is in accordance with the expected function of the dedicated damping term in (24). In addition, although the parameters of VSG2 do not influence K_J and K_D, they can still participate in the dynamics of VSG1 by K_S.

As mentioned above, this section presents an example to analyze the role of a dedicated damping term. There are still other dedicated damping strategies proposed in the literature. Although it is not possible to include them all in the paper, they can be analyzed by a similar process.

D. Application in large power system

The aforementioned conclusions can effectively be applied to a larger power system with multiple VSGs. Fig. 11(a) presents a general power system with N VSGs, where VSG1 is assumed as the studied unit. If the system can be reduced to an equivalent paralleled system shown in Fig. 11(b), where H_a, D_{pa}, and X_a are the aggregated parameters of the reduced part, it is similar with the investigated system of this paper. On one hand, several aggregation methods of the generating units may be used to achieve this goal such as in [34] and [35]. The accurate aggregation method is still an open topic but not the key point of this paper. On the other hand, even if the accurate values of the aggregated model cannot be obtained, the conclusions of this paper can still provide a qualitative analysis. Taking the input changing as an example, according to the analysis based on the equivalent coefficients, the equivalent inertia and damping characteristics of VSG1 are only determined by H_1 and D_{p1}, while the aggregated coefficients H_a, D_{pa}, and X_a do not influence K_J and K_D of VSG1. Meanwhile, H_a, D_{pa}, and X_a should be determined by the structure of the network and other VSGs (i.e., VSG2 - VSGN). Therefore, it can be concluded that the structure of the network and parameters of other VSGs will not affect the equivalent inertia and damping characteristics of VSG1. When focusing on other VSGs rather than VSG1, similar analysis can

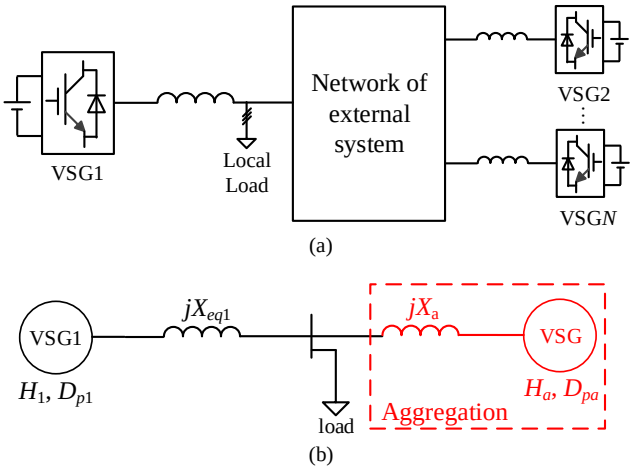

Fig. 11. Model aggregation of power system. (a) General diagram of power system. (b) Reduced power system after aggregation.

be made. Besides, if the power system can be reduced to two paralleled area, the conclusions in this paper can be used as well.

E. Discussion

Compared to the traditional power system, the power converter based system may suffer from a high risk of frequency oscillation. Nevertheless, the indices such as RoCoF and nadir can still be used to evaluate a power system with power converter based generators, e.g., VSGs. Especially, the RoCoF at the beginning of the disturbance is of great importance. These indices are highly related to the inertia and damping characteristics of VSGs connected in the power system. The aforementioned equivalent coefficients analysis shows which parameters and how they will influence the inertia and damping characteristics of a VSG under different disturbances. Therefore, the equivalent coefficients provide a guide to improve the performance of a VSG by appropriately choosing and adjusting the parameters without changing the control structure. For example, if a VSG shows a big RoCoF following a load disturbance, it can be, from the equivalent inertia coefficient, improved by increasing its inertia constant or virtual impedance. However, for a reference step, the virtual impedance has no contribution to the equivalent inertia coefficient, and therefore, cannot be chosen as an adjustable parameter in order to improve the RoCoF. Meanwhile, the equivalent synchronizing coefficient implies that it is possible to achieve better dynamics by changing parameters of other VSGs without influencing the RoCoF of the focused VSG. The next section shows a simple application to achieve better dynamics to both load step and reference step.

IV. Modified Inertia Control for Enhanced Transient Response

A. Control strategy

In order to obtain the identical equivalent inertia and damping characteristics for the parallel VSGs, (23) should be satisfied, which is preferable for the transient power sharing

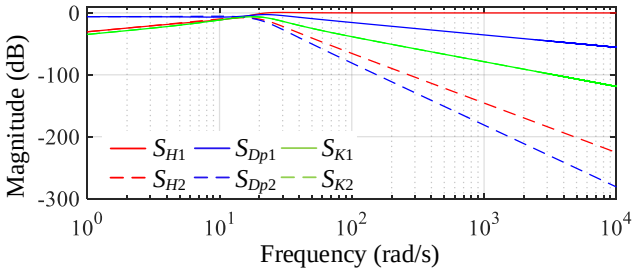

Fig. 12. Sensitivities of system to variations of parameters.

under load disturbances. However, this condition may not be in accordance with the requirement when the set-point changes such as in the secondary control. Actually, like the SG in the traditional power system, it is not necessary that all the VSGs should participate in the secondary control. As aforementioned discussion, the RoCoF is an important index for the frequency stability, which is highly related to the inertia of the system. As in (16), it is better to have a larger virtual inertia for the VSGs, which has reserve capacity to take part in the secondary control in order to keep the frequency more stable.

In the proposed modified virtual inertia control, the inertia constant of the VSG participating in the secondary control is a function of ΔP_0 given as the following

$$H = H_{small} + sgn(|\Delta P_0|)(H_{large} - H_{small}) \tag{26}$$

where $sgn()$ represents the sign function. As seen, only when the primary control is in action, i.e., $\Delta P_0 = 0$, $sgn() = 0$, and therefore $H = H_{small}$, which is the inertia constant for the load disturbance. When the secondary control requires the VSG to provide more power, i.e., $\Delta P_0 > 0$, $sgn() = 1$, and therefore $H = H_{large}$, which is a large inertia constant for the variation of the set-point. When the system comes into a new steady-state after the variation of the set-point, ΔP_0 will be reset to zero, which makes $H = H_{small}$ again. The paralleled VSGs will share the load disturbance until a new set-point is sent.

B. Sensitivity and Stability analysis

To further prove the effectiveness of the proposed method, Fig. 12 shows the system sensitivities to the change of parameters, which are defined as [36]

$$S_\rho = \frac{\partial T}{\partial \rho}\frac{\rho}{T} \tag{27}$$

where T is the transfer function from ΔP_{0_1} to $\Delta\omega_1^*$, ρ is the studied parameter. As shown, S_{H1} has the highest value in the high-frequency domain, which implies that the gain of the system in the high-frequency domain is more sensitive to the variation of H_1. Therefore, it is possible to limit the quick dynamics of $\Delta\omega_1^*$, i.e., the RoCoF, by H_1, which means that they can hardly influence the RoCoF.

Thereafter, the available H_{large} should be determined. According to Fig. 8, the small-signal model of the parallel VSGs system is

$$\dot{\boldsymbol{x}} = \boldsymbol{A}\boldsymbol{x} + \boldsymbol{B}\boldsymbol{u} \tag{28}$$

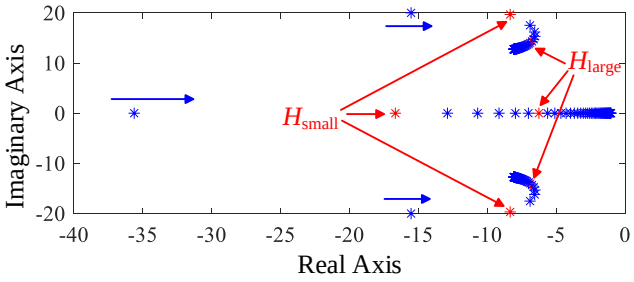

Fig. 13. Loci when H_1 increases from 1 s to 100 s.

where

$$\boldsymbol{x} = [\Delta\omega_1^*,\ \Delta\omega_2^*,\ \Delta\delta_1 - \Delta\delta_2]^T,\ \boldsymbol{u} = [\Delta P_{0\_1},\ \Delta p_l^*]^T \tag{29}$$

$$\boldsymbol{A} = \begin{bmatrix} -\frac{1}{2H_1 D_{p1}} & 0 & -\frac{K_1 K_2}{2H_1(K_1+K_2)} \\ 0 & -\frac{1}{2H_2 D_{p2}} & \frac{K_1 K_2}{2H_2(K_1+K_2)} \\ \omega_n & -\omega_n & 0 \end{bmatrix} \tag{30}$$

$$\boldsymbol{B} = \begin{bmatrix} \frac{1}{2H_1} & 0 & 0 \\ -\frac{K_1}{2H_1(K_1+K_2)} & -\frac{K_2}{2H_2(K_1+K_2)} & 0 \end{bmatrix}^T \tag{31}$$

Fig. 13 shows the loci when H_1 increases from 1 s to 100 s. This figure only reflects the poles of the system without considering the impact of the zeros. However, the feasible parameters should guarantee the stability preferentially. As seen, the system is always stable with the used parameters in this paper. When choosing H_{small}, the relationship of (23) should be firstly considered. When choosing H_{large}, a large values is expected in order to improve the inertia characteristics. However, a large H makes the loci move closely to the imaginary axis, which implies a smaller stability margin and slower response speed. Therefore, a compromise is needed, where H_{large} is chosen as 5 times of H_{small} in this paper. If multiple dynamic requirements should be exactly achieved simultaneously, some additional control terms may be added, which is not the purpose of this paper.

V. Experimental Validation

The prototype is established in the lab to verify the analysis and the proposed method, where the setup of the experimental system is shown in Fig. 14. The power converter system is based on Danfoss inverter, and the control is executed by the DS1007 dSPACE system. The main parameters of the test system are listed in Table I, which is used in all of the experiment conditions if there is no specific illustration. The changeable parameters are shown in the corresponding experimental figures and the other parameters are identical for a fair comparison.

At beginning, Fig. 15 gives the comparisons between the small-signal model and the experimental results with a 2.5 kW load step, which verifies the correctness of the small-signal model. Meanwhile, it proves that neglecting the quick dynamics of the double loop and the power stage is reasonable. Therefore, in the following part, the equivalent coefficients are analyzed and verified by using the experimental results. In order to highlight the benefits of the VSG control, the

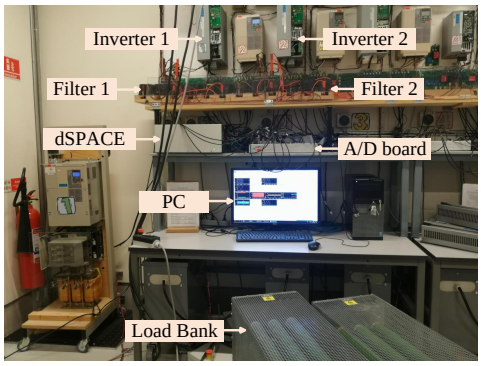

Fig. 14. Setup of experimental system with two paralleled inverters.

TABLE I
Key Parameters of Experimental Setup

Parameter	Value	Parameter	Value	Parameter	Value
f_n	50 Hz	V_n	380 V	H_i	3 s
L_{fi}	3 mH	f_{sw}	10 kHz	D_{pi}	0.01
C_{fi}	10 μF	ω_0	100π rad/s	X_{vi}	3 Ω
L_{si}	1 mH	V_0	320 V	S_{ni}	5 kW

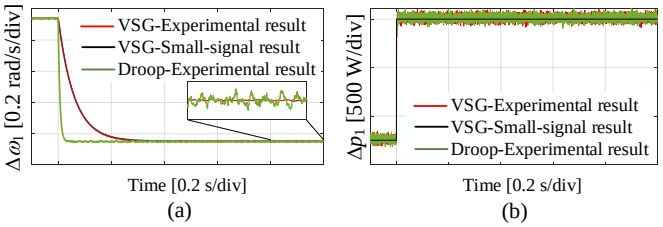

Fig. 15. Validation of small-signal model. (a) Frequency. (b) Active power.

experimental results of the traditional droop control with virtual impedance are also presented in Fig. 15. It shows that the frequency of droop control has more high-frequency oscillations. Besides, the VSG and droop control have the same steady-state frequency deviations. However, it can be calculated that the RoCoF of the droop control after the disturbance is 1.1 Hz/s, which is larger than the limitations both in IEEE Std 1547-2018 and the recommended new value in Ireland. In contrast, the RoCoF of the VSG is only 0.16 Hz, which is well acceptable.

A. Equivalent inertia and damping characteristics

1) Variation of P_{0_1}: The dynamics of the parallel VSGs system is studied when P_{0_1} steps from 2.5 kW to 5 kW.

As it is shown in Fig. 16(a), as H_1 becomes larger, the RoCoF of VSG1 at the beginning of the disturbance is decreased. As a result, the maximum frequency deviation and the oscillatory frequency decrease as well. The response speed of the output active power of VSG1 is also decreased. Therefore, it can be concluded that the inertia characteristics of VSG1 when the disturbance occur is enhanced by a larger H_1. In comparison, as illustrated in Fig. 16(b), the effects of H_2 are quite different. On one hand, focusing on the beginning of the disturbance, the dynamics are almost identical with different

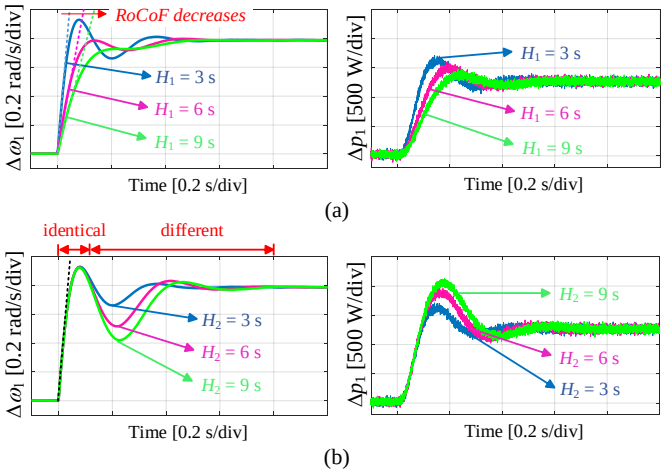

Fig. 16. Experimental results of frequency and active power of VSG1 when P_{0_1} changes under different inertia constants (a) H_1, (b) H_2.

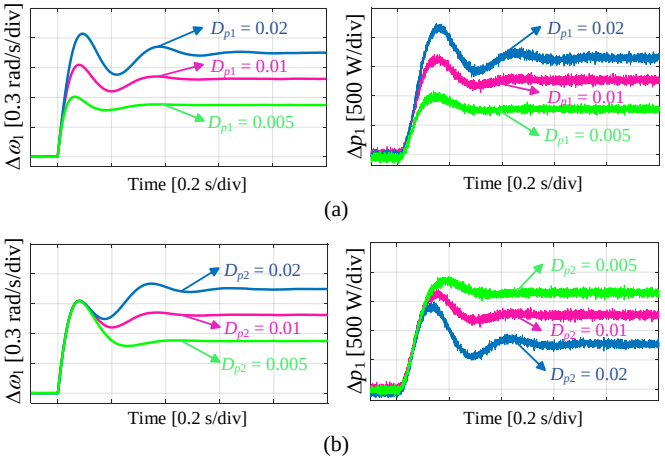

Fig. 17. Experimental results of frequency and active power of VSG1 when P_{0_1} changes under different droop coefficients (a) D_{p1}, (b) D_{p2}.

H_2, especially the RoCoF and maximum frequency deviation. It implies that the inertia and damping characteristics are not changed by H_2. Corresponding to the equivalent coefficients, the aforementioned results are due to that H_2 has almost no impact on K_J and K_D of VSG1 in this case. On the other hand, focusing on the stage after about the first peak, the dynamics with different H_2 become quite different among each other. Specifically, as H_2 increases, the system becomes more oscillatory with a smaller frequency, which implies a longer time in order to reach the steady-state. Meanwhile, a smaller transient frequency will be observed, and therefore a larger transient power is provided as H_2 increases. These findings reflect that K_S begins to take action in this stage. Corresponding to the equivalent coefficient, it implies that H_2 does can change K_S as given in (16). In summary, H_1 will change the inertia characteristics responding to a disturbance in P_{0_1}, while H_2 cannot. Nevertheless, H_2 will influence the synchronization and how the system goes into the steady-state.

As shown in Fig. 17, a smaller D_{p1} damps the oscillatory magnitude of the frequency and the output power at the beginning of the transient without changing the RoCoF, which implies better damping characteristics. However, the oscillatory magnitude of the frequency and the output power can hardly be changed by the variations of D_{p2} as shown in Fig. 17(b), and this proves that D_{p2} has a small impact on the damping characteristics of VSG1. However, D_{p2} will influence the dynamics of by changing K_S as well. A smaller D_{p2} leads to a more stable system. It is also illustrated that both droop coefficients will have an impact on the steady-state.

Fig. 18 shows the impact of the virtual impedances. As seen, the RoCoF, the oscillatory magnitudes of the frequency and the output power are all changing a little, which implies similar inertial and damping characteristics, and the differences of the dynamics come from the variations of K_S due to different virtual impedances leading to different K_i. From (16), K_1 and K_2 have the same impact on K_S, and therefore, the dynamics in Fig. 18(a) and (b) are almost identical.

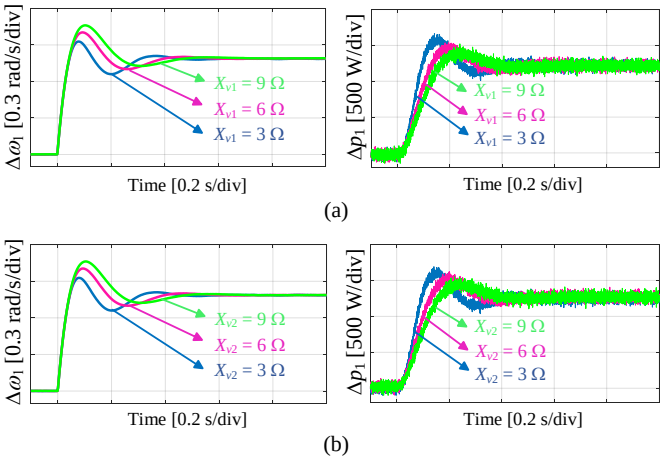

Fig. 18. Experimental results of frequency and active power of VSG1 when P_{0_1} changes under different virtual impedances (a) X_{v1}, (b) X_{v2}.

2) Load disturbance: The dynamics of the parallel VSGs system is studied by making a load step of 2.5 kW.

Fig. 19 illustrates the response of VSG1 when there is a load step under different inertial constants. As seen, both of H_1 and H_2 will influence the dynamics, which is attributed to the transient power unbalance due to the difference of the parameters. However, it is obvious that the impacts of H_1 and H_2 are quite different. In this paper, it is shown that the physical essence is the difference of the equivalent inertia when there is a load disturbance. According to (19), a larger H_1 implies a larger equivalent inertia. Therefore, the increase of H_1 will significantly decrease the RoCoF of VSG1 at the beginning of the disturbance, while variations of H_2 does not change the RoCoF in comparison. However, H_2 will influence the dynamics coming into the steady-state. Meanwhile, the settling time of the system depends on the VSG with a larger inertial constant. It is also shown from the waveforms of the active power that the VSG with a larger inertial constant will provide more power during the dynamics.

Fig. 20 illustrates the response of VSG1 under a load step

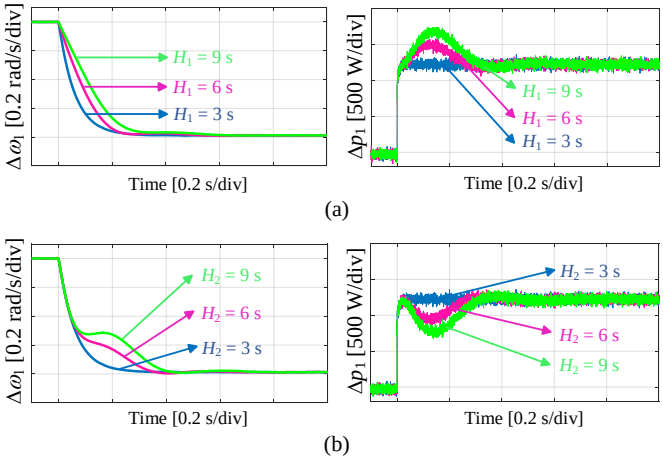

Fig. 19. Experimental results of frequency and active power of VSG1 when load steps under different inertia constants (a) H_1, (b) H_2.

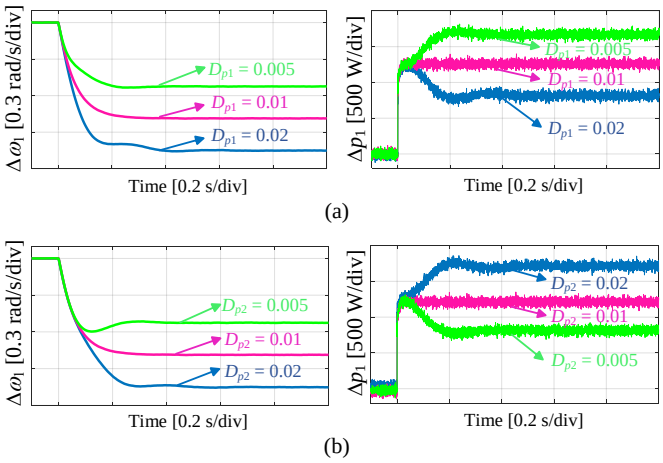

Fig. 20. Experimental results of frequency and active power of VSG1 when load steps under different droop coefficients (a) D_{p1}, (b) D_{p2}.

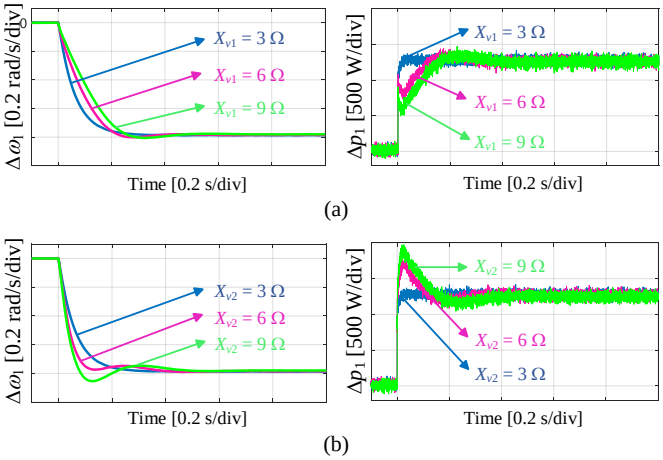

Fig. 21. Experimental results of active power and frequency of VSG1 when load steps under different virtual impedances (a) X_{v1}, (b) X_{v2}.

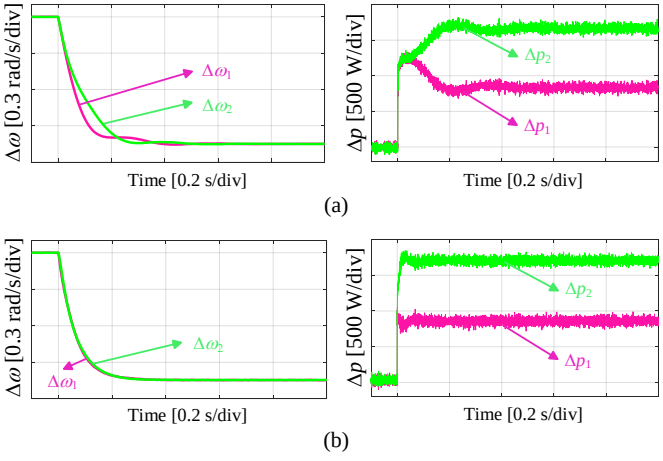

Fig. 22. Experimental results of transient power sharing when (a) Eq. (23) is not satisfied, (b) Eq. (23) is satisfied.

with different droop coefficients. By comparing the waveforms of the angle frequency, it can be seen that increasing D_{p1} significantly changes the oscillatory magnitude of the frequency, while changing D_{p2} influences the damping characteristics of VSG1 slightly.

Fig. 21 shows the impact of the virtual impedances on the dynamics of VSG1. In order to have a better understanding, the results are compared with Fig. 18. As seen, the variations of the virtual impedances can also influence the RoCoF when the disturbance occurs, which is not observed in Fig. 18. This is because, as given in (19), the virtual impedance will change the equivalent inertia by influencing K_1 and K_2. In comparison, as in (16), K_J is independent on the virtual impedances. Therefore, the term $(K_1+K_2)/K_1$ in the equivalent coefficients represents how the impedances will affect the dynamics of VSG1. Meanwhile, it is also illustrated in Fig. 21 that the impact of X_{v2} on the inertial and the damping characteristics are just opposite with those shown in X_{v1}.

3) Transient power sharing: In this part, the condition of (23) for the transient power sharing is verified. First, it is supposed that $H_1/H_2 = X_{v1}/X_{v2} = 1$, $D_{p1}/D_{p2} = 2$, and the experimental results are shown in Fig. 22(a). As seen, the transient power is not shared properly and large oscillations can be observed when there is a load step. Then H_2 and X_{v2} are changed to satisfy (23), and the experimental results are given in Fig. 22(b), which shows that the dynamics is highly improved. It is worth noting that there are still small oscillations in the dynamics of the parallel VSGs. This is because that K_1 and K_2 are not only related to X_{v1} and X_{v2}, but also related to the steady-state operational point and line impedance. As mentioned in Section III-C-3), the exact values of line impedance are hard to know. Although the same line parameters are chosen in the experiments, the actual values may still have errors. In addition, there may be errors introduced by the experiments as well. All the aforementioned factors will influence the exact satisfaction of (23).

B. Improved inertia control

In this section, the set-point of VSG1 is supposed to be able to change in order to meet the requirement of the

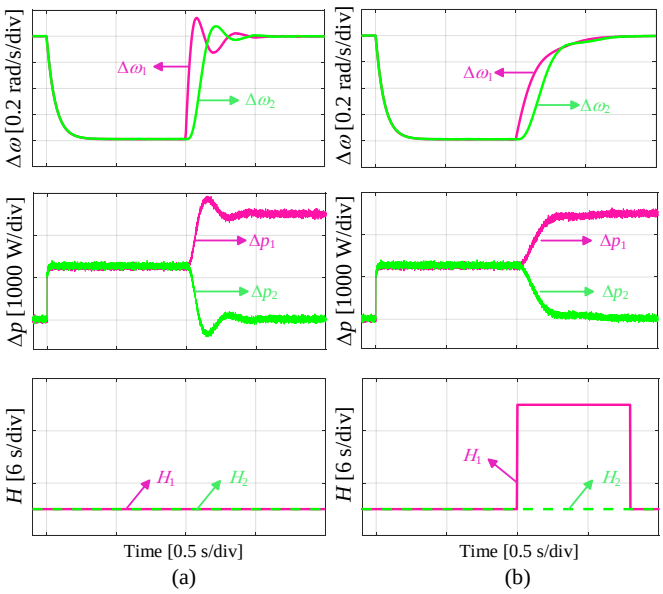

Fig. 23. Experimental results of frequency, active power, and inertia constant of VSGs controlled by (a) basic VSG control, (b) proposed inertia control.

TABLE II
COMPARISONS OF ROCOF AND FREQUENCY DEVIATION WITH BASIC VSG AND WITH PROPOSED INERTIA CONTROL

	RoCoF		Frequency deviation	
	$\Delta\omega_1$	$\Delta\omega_2$	$\Delta\omega_1$	$\Delta\omega_2$
Basic VSG Control	1.4 Hz/s	0.6 Hz/s	0.02 Hz	0.01 Hz
Proposed Control	0.7 Hz/s	0.2 Hz/s	0 Hz	0 Hz

operation such as the secondary control. First, a 2.5 kW load step is applied, and then the set-point of VSG1 changes to restore the frequency. As seen in Fig. 23, both the traditional VSG control and the proposed improved inertia control can guarantee a good performance response to a load step because they have the identical parameters. However, this will lead to a large oscillation when P_{0_1} changes as shown in Fig. 23(a). In comparison, H_1 automatically becomes 5 times to 15 s responding to the increasing of P_{0_1} in the proposed controller. As a result, as shown in Fig. 23(b), the oscillations in both the frequencies and active powers can be obviously decreased during the transient process. After 0.8 s, H_1 returns to 3 s.

As mentioned before, the RoCoF and frequency deviation with respect to the steady-state value can be used to evaluate the frequency of the system. Therefore, Table II shows the comparison results with the basic VSG control and with the proposed inertia control, which illustrates that the RoCoF are decreased by the proposed method. Meanwhile, the frequency deviations become 0 Hz, which means there are no overshoots in these frequencies.

VI. CONCLUSION

In this paper, the inertia and damping characteristics of the parallel VSGs are investigated by the equivalent coefficients. Both the load disturbance and variation of the set-point are considered. The conclusions are given as following.

1) When there is a load disturbance or the set-point of VSG changes, the inertia and damping characteristics of a VSG are influenced by the parameters of itself, but are independent on other VSGs'. Especially, enlarging the inertia constants of other VSGs' will hardly improve the RoCoF of the local VSG.
2) With a load disturbance, the inertia and damping characteristics are related to the impedances of the power system. In order to achieve power sharing, the ratio of the corresponding parameters in p.u. values should be identical.
3) The proposed enhanced inertia control strategy can improve the frequency performance of the parallel VSGs.

The analysis in this paper assumes an inductive equivalent impedance (e.g., with the help of virtual reactance), which may therefore not suitable to a completely resistive network.

REFERENCES

[1] J. Fang, H. Li, Y. Tang, and F. Blaabjerg, "On the inertia of future more-electronics power systems," *IEEE J. Emerg. Sel. Top. Power Electron.*, vol. 7, no. 4, pp. 2130–2146, Dec. 2019.
[2] W. Zhang, J. Rocabert, J. I. Candela, and P. Rodriguez, "Synchronous power control of grid-connected power converters under asymmetrical grid fault," *Energies*, vol. 10, no. 7, pp. 1–21, Jul. 2017.
[3] J. Rong, X. Ai, Y. Li, and D. Ren, "Research on the structure and control strategy of a novel power electronic transformer for AC/DC hybrid distribution network," *Appl. Sci.*, vol. 9, no. 4, pp. 1–20, Feb. 2019.
[4] M. Karimi-Ghartemani, S. A. Khajehoddin, P. Piya, and M. Ebrahimi, "Universal controller for three-phase inverters in a microgrid," *IEEE J. Emerg. Sel. Top. Power Electron.*, vol. 4, no. 4, pp. 1342–1353, Dec. 2016.
[5] J. Liu, Y. Miura, and T. Ise, "Comparison of dynamic characteristics between virtual synchronous generator and droop control in inverter-based distributed generators," *IEEE Trans. Power Electron.*, vol. 31, no. 5, pp. 3600–3611, May 2016.
[6] M. Chen and X. Xiao, "Hierarchical frequency control strategy of hybrid droop/VSG-based islanded microgrids," *Electr. Power Syst. Res.*, vol. 155, pp. 131–143, Feb. 2018.
[7] IEEE PES Power System Dynamic Performance Committee, "Stability definitions and characterization of dynamic behavior in systems with high penetration of power electronic interfaced technologies," Tech. Rep., 2020.
[8] IEEE Standard Association, *IEEE Std. 1547-2018. Standard for Interconnection and Interoperability of Distributed Energy Resources with Associated Electric Power Systems Interfaces*, 2018.
[9] P. Tielens and D. Van Hertem, "The relevance of inertia in power systems," *Renew. Sustain. Energy Rev.*, vol. 55, no. 2016, pp. 999–1009, Mar. 2016.
[10] W. He, X. Yuan, and J. Hu, "Inertia provision and estimation of PLL-based DFIG wind turbines," *IEEE Trans. Power Syst.*, vol. 32, no. 1, pp. 510–521, Jan. 2017.
[11] R. K. Panda, A. Mohapatra, and S. C. Srivastava, "An effective inertia control scheme for solar PV systems with conventional dq controller," in *2018 IEEE Power Energy Soc. Gen. Meet.*, pp. 1–5.
[12] Y. Wu, D. Zhang, L. Xiong, S. Wang, Z. Xu, and Y. Zhang, "Modeling and mechanism investigation of inertia and damping issues for grid-tied PV generation systems with droop control," *Energies*, vol. 12, no. 10, pp. 1–17, May 2019.
[13] S. Tan, H. Geng, G. Yang, H. Wang, and F. Blaabjerg, "Modeling framework of voltage-source converters based on equivalence with synchronous generator," *J. Mod. Power Syst. Clean Energy*, vol. 6, no. 6, pp. 1291–1305, Nov. 2018.
[14] A. D. Paquette, M. J. Reno, R. G. Harley, and D. M. Divan, "Sharing transient loads : causes of unequal transient load sharing in islanded microgrid operation," *IEEE Ind. Appl. Mag.*, vol. 20, no. 2, pp. 23–34, Mar. 2014.
[15] R. Rosso, S. Engelken, and M. Liserre, "Robust stability analysis of synchronverters operating in parallel," *IEEE Trans. Power Electron.*, vol. 34, no. 11, pp. 11 309–11 319, Nov. 2019.

[16] Z. Wang, F. Zhuo, H. Yi, J. Wu, F. Wang, and Z. Zeng, "Analysis of dynamic frequency performance among voltage-controlled inverters considering virtual inertia interaction in microgrid," *IEEE Trans. Ind. Appl.*, vol. 55, no. 4, pp. 4135–4144, Jul. 2019.
[17] Z. Wang, H. Yi, F. Zhuo, J. Wu, and C. Zhu, "Analysis of parameter influence on transient active power circulation among different generation units in microgrid," *IEEE Trans. Ind. Electron.*, vol. 68, no. 1, pp. 248–257, Jan. 2021.
[18] Z. Wang, F. Zhuo, J. Wu, H. Yi, H. Zhai, and Z. Zeng, "Inertia time constant design in microgrids with multiple paralleled virtual synchronous generators," in *2017 19th Eur. Conf. Power Electron. Appl. (EPE'17 ECCE Eur.)*, pp. 1–9.
[19] H. Xu, X. Zhang, F. Liu, R. Shi, C. Yu, and R. Cao, "A reactive power sharing strategy of VSG based on virtual capacitor algorithm," *IEEE Trans. Ind. Electron.*, vol. 64, no. 9, pp. 7520–7531, Sep. 2017.
[20] X. Yan, A. Rasool, F. Abbas, H. Rasool, and H. Guo, "Analysis and optimization of the coordinated multi-VSG sources," *Electronics*, vol. 8, no. 1, pp. 1–22, Dec. 2018.
[21] J. Liu, Y. Miura, H. Bevrani, and T. Ise, "Enhanced virtual synchronous generator control for parallel inverters in microgrids," *IEEE Trans. Smart Grid*, vol. 8, no. 5, pp. 2268–2277, Sep. 2017.
[22] J. Liu, Y. Miura, H. Bevrani, and T. Ise, "A unified modeling method of virtual synchronous generator for multi-operation-mode analyses," *IEEE J. Emerg. Sel. Top. Power Electron.*, 2020.
[23] Z. Shuai, W. Huang, Z. J. Shen, A. Luo, and Z. Tian, "Active power oscillation and suppression techniques between two parallel synchronverters during load fluctuations," *IEEE Trans. Power Electron.*, vol. 35, no. 4, pp. 4127–4142, Apr. 2020.
[24] M. Chen, D. Zhou, and F. Blaabjerg, "Characteristics of virtual synchronous generator based voltage source converter," in *2020 IEEE Power Energy Soc. Gen. Meet.*, pp. 1–5.
[25] T. Shintai, Y. Miura, and T. Ise, "Oscillation damping of a distributed generator using a virtual synchronous generator," *IEEE Trans. Power Deliv.*, vol. 29, no. 2, pp. 668–676, Apr. 2014.
[26] S. Dong and Y. C. Chen, "Adjusting synchronverter dynamic response speed via damping correction loop," *IEEE Trans. Energy Convers.*, vol. 32, no. 2, pp. 608–619, Jun. 2017.
[27] J. Alipoor, Y. Miura, and T. Ise, "Power system stabilization using virtual synchronous generator with alternating moment of inertia," *IEEE J. Emerg. Sel. Top. Power Electron.*, vol. 3, no. 2, pp. 451–458, Jun. 2015.
[28] D. Li, Q. Zhu, S. Lin, and X. Y. Bian, "A self-adaptive inertia and damping combination control of VSG to support frequency stability," *IEEE Trans. Energy Convers.*, vol. 32, no. 1, pp. 397–398, Mar. 2017.
[29] F. Wang, L. Zhang, X. Feng, and H. Guo, "An adaptive control strategy for virtual synchronous generator," *IEEE Trans. Ind. Appl.*, vol. 54, no. 5, pp. 5124–5133, Sep. 2018.
[30] P. Kundur, *Power system stability and control*. McGraw-Hill, 1993.
[31] J. Rocabert, A. Luna, F. Blaabjerg, and P. Rodríguez, "Control of Power Converters in AC Microgrids," *IEEE Trans. Power Electron.*, vol. 27, no. 11, pp. 4734–4749, nov 2012.
[32] H. Wu and X. Wang, "A mode-adaptive power-angle control method for transient stability enhancement of virtual synchronous generators," *IEEE J. Emerg. Sel. Top. Power Electron.*, vol. 8, no. 2, pp. 1034–1049, Jun. 2020.
[33] O. Mo, S. D'Arco, and J. A. Suul, "Evaluation of virtual synchronous machines with dynamic or quasi-stationary machine models," *IEEE Trans. Ind. Electron.*, vol. 64, no. 7, pp. 5952–5962, Jul. 2017.
[34] J. Machowski, J. W. Bialek, and J. R. Bumby, *Power System Dynamics: Stability and Control*. Wiley, 2008.
[35] X. Yu, K.-J. Li, M. Wang, Z.-d. Wang, K. Sun, and J. Lou, "A multistep dynamic equivalent method for urban power grid based on district dividing," *IEEE Trans. Ind. Appl.*, vol. 53, no. 2, pp. 908–917, Mar. 2017.
[36] R. C. Dorf and R. H. Bishop, *Modern Control Systems*. Prentice Hall, 2011.